Three-Dimensional Vibrational Imaging of a Microcrystalline J-Aggregate Using Supercontinuum-Based Ultra-Broadband Multiplex Coherent Anti-Stokes Raman Scattering Microscopy

Hideaki Kano* and Hiro-o Hamaguchi

Department of Chemistry, School of Science, The University of Tokyo, Hongo 7-3-1, Bunkyo, Tokyo 113-0033, Japan

Received: November 21, 2005; In Final Form: January 3, 2006

Vibrational properties of a porphyrin J-aggregate microcrystal have been investigated by ultra-broadband multiplex coherent anti-Stokes Raman scattering (CARS) microspectroscopy using a supercontinuum light source generated from a photonic crystal fiber. Owing to a strong resonance effect due to an excitonic transition, clear spectral and spatial profiles of the CARS signal have been successfully obtained. On the basis of the comparison between the CARS and the fluorescence images, the spatial dependence of the CARS signal can be explained by the spatial inhomogeneity of the excitonic transition energy in the single J-aggregate microcrystal.

1. Introduction

Molecular J-aggregates have been attracting much scientific interest because they are regarded as a model material for one-dimensional molecular excitons.[1−3] J-aggregates exhibit various unique optical properties such as sharp absorption, the so-called J-band, and ultrafast response due to the exciton superradiance.[2,4] Especially, J-aggregates composed of porphyrin derivatives have been widely studied[5−17] in connection with the light-harvesting and primary charge-separation events of photosynthesis. Among several water-soluble porphyrin derivatives, tetraphenylporphinesulfonate (TPPS) J-aggregates have been intensively investigated to elucidate the excitonic property, the ultrafast response in the excited state, and the delocalization size of the exciton in J-aggregates.[5−17]

Recently, the formation of J-aggregates and their microcrystals have been reported for water-insoluble porphyrin derivatives at the liquid−liquid or gas−liquid interface by Okada and Segawa.[18] They have also reported that the absorption peak position due to the S_1-exciton transition (Q-band) is controllable by changing the meso-substituents of a porphyrin monomer. To elucidate this absorption change, it is important to examine not only the electron-donating character of the meso-substituents and the configuration of the monomers in the aggregate[18] but also the perturbation of the vibronic interaction between the Q and B band (S_2-exciton band or Soret band) due to the meso-substituents, because the optical transition to the Q-band is allowed by the vibronic interaction through the B band.[19] Raman microspectroscopy is one of the most powerful methods that allow us to investigate the vibronic character and reveal the polymorphism of microcrystalline J-aggregates in detail. Although several reports have been made of atomic force microscopy (AFM),[18] time-resolved near-field spectroscopy,[20,21] and third-harmonic generation[22] on the microcrystalline J-aggregates, only a few studies have been reported by Raman microspectroscopy.[23,24] In particular, the resonance Raman microscopic study at the Q-band has not been reported except the study by our group.[25] It is probably due to the high quantum yield of the one-photon fluorescence from the Q-band. The spontaneous Raman signal is often overwhelmed by such a strong fluorescence signal. On the contrary, nonlinear Raman microspectroscopy such as coherent anti-Stokes Raman scattering (CARS) microspectroscopy can be used to avoid a broad background due to the one-photon fluorescence, because the Raman signal is detected at the wavelength shorter than those of the incident lasers. In addition to the fluorescence-free detection, the CARS process can boost the weak Raman signal by coherent vibrational excitation. Therefore, CARS microspectroscopy is expected to be one of the most promising methods to study the vibrational properties of J-aggregate microcrystals.

CARS is one of the third-order nonlinear optical processes. A particular Raman transition is coherently driven by two lasers, namely pump and Stokes laser pulses. Subsequently, vibrational coherence due to a Raman transition is probed by the pump laser pulse, giving rise to a CARS signal. Recently, significant progress has been made of CARS microscopy.[26−40] Especially, ultra-broadband multiplex CARS microspectroscopy has been developed using a photonic crystal fiber (PCF)[25,38−41] and a tapered fiber.[36] Both PCF and tapered fiber enable us to generate a supercontinuum using an unamplified Ti:Sapphire oscillator.[42,43] The supercontinuum as the Stokes laser pulse significantly broadened the spectral coverage to more than 2800 cm^{-1}.[41] In the present study, we have applied supercontinuum-based ultra-broadband multiplex CARS microspectroscopy to microcrystalline J-aggregates and investigated the vibrational as well as excitonic properties.

2. Experimental Section

A. Ultra-Broadband Multiplex CARS Microspectroscopy. The ultra-broadband multiplex CARS microspectroscopy using a PCF has been described elsewhere.[38,39,41] The light source is an unamplified mode-locked Ti:Sapphire oscillator (Coherent, Vitesse-800), producing 100 fs pulses at 800 nm, with a repetition rate of 80 MHz. After passing through an optical isolator, about 80% of the oscillator output was used as

* Corresponding author. E-mail: hkano@chem.s.u-tokyo.ac.jp.

10.1021/jp056749j CCC: $33.50
Published on Web 02/02/2006

the pump laser (ω_1). To obtain a Raman spectrum with a high frequency resolution, the pump pulse was spectrally filtered by a narrow band-pass filter. The peak position and bandwidth were measured to be about 12 500 cm^{-1} (800 nm) and 20 cm^{-1}, respectively. The remaining laser output was used for the seed laser to generate the supercontinuum in the PCF (Crystal Fibre, NL-PM-750). The near-infrared (NIR) component of the supercontinuum was used for the Stokes light (ω_2), because the wavelength of the pump laser was also in the NIR region. In the previous study,[38,39] the optimized delay time between the pump and Stokes pulses was different for different vibrational modes due to the small negative chirp of the Stokes pulses. In the present setup, we have compensated the temporal chirp of the Stokes pulses by controlling the length of the PCF.[41] Owing to the balance between the fiber dispersion and the material dispersion due to the optics, the temporal width of the Stokes pulse is decreased to be less than 1 ps. The pump and Stokes pulses are combined collinearly with an 800 nm Notch filter and then tightly focused onto the sample with a 40× microscope objective. To avoid the damage of the sample, the pulse energy of the incident lasers was decreased to be 80 and 104 pJ for the pump and the Stokes lasers, respectively. The forward-propagating CARS signal was collected with another 40×, 0.6 NA microscope objective. After passing through an 800 nm Notch and short-wavelength pass filters, the CARS signal was spectrally dispersed by a polychromator (Acton, SpectraPro-300i) and detected by a CCD camera (Roper Scientific, Spec-10:400BR/XTE). The spectral coverage of the CARS signal is more than 2800 cm^{-1} in the present setup. Because the chirp in the supercontinuum is negligible in the present setup,[44] the overall spectral resolution was determined mainly by the grating in the polychromator and was estimated to be 38 cm^{-1}. The grating with 300 grooves was chosen in the present study for simultaneous measurement of the CARS and fluorescence signals. The multiplex CARS images were measured by a point-by-point acquisition of the CARS signal. The sample was scanned by a piezo-driven *xyz* translator (MadCity, Nano-LP-100). The spatial resolution was estimated to be 0.47 ± 0.01 μm for the lateral and 1.51 ± 0.02 μm for the axial directions, respectively, by measuring a small J-aggregate microcrystal. The exposure time for each point was 60 ms.

B. Sample Preparation. A microcrystal of *meso*-tetraphenylporphyrin (TPP, Figure 1a) was used as the sample. TPP was purchased from Wako Pure Chemicals and was used without further purification. The J-aggregate assembly composed of the water-insoluble TPP monomers was formed using a method similar to that reported by Okada and Segawa.[18] A few drops of a CH_2Cl_2 solution of TPP were added into aqueous sulfuric acid (20% (w/w)). The concentration of the TPP solution was about 10^{-5} M. The J-aggregate assembly was taken out of the solution and was placed on a slide glass. The proposed structure of the porphyrin J-aggregate is shown in Figure 1b.[18] Another model based on an AFM study has also been proposed.[45] Figure 1c shows a microscopic image of the J-aggregate microcrystal, which is obtained by a 40× microscope objective. Many platelike green microcrystals are clearly observed. Owing to the quasi-one-dimensional aggregation of TPP molecules (See Figure 1b), the microcrystal seems to grow in a unidirectional way on the surface of aqueous sulfuric acid.

3. Results and Discussion

A. Absorption and CARS Spectra. Figure 2 shows a typical absorption spectrum of the microcrystalline TPP J-aggregates, which is obtained by the illumination lamp attached to the microscope. The spectral profile is spatially averaged. The absorption spectrum of the J-aggregate microcrystal shows an intense absorption peak at 722 nm. It corresponds to the transition from the ground state to the S_1-exciton state (Q-band), which is red-shifted from the absorption peak position of the TPP monomer. In the present setup, the center wavelength of the pump laser is about 800 nm. Therefore, a strong excitonic resonance effect is expected to take place in the CARS process. Figure 3a shows typical CARS spectra at zero (solid, hatched with dark gray) and −13.3 ps (dotted, hatched with light gray) delay times between the pump and Stokes pulses. In the present condition, the zero delay time was determined by the maximum

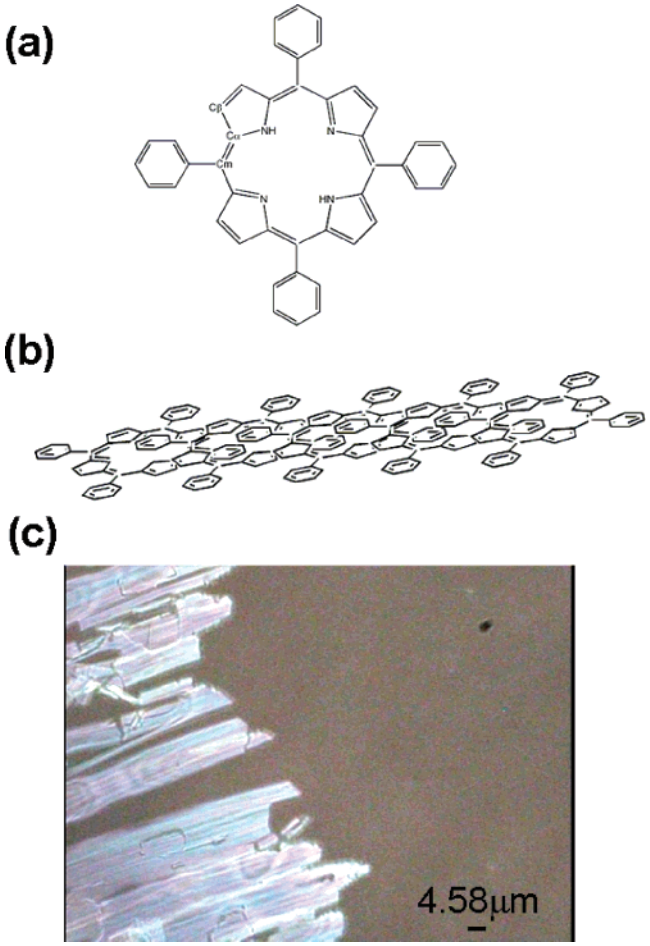

Figure 1. (a) Molecular structure of *meso*-tetraphenylporphyrin (TPP). (b) Proposed structure of the porphyrin J-aggregate. (c) Microscopic image of TPP J-aggregate microcrystals.

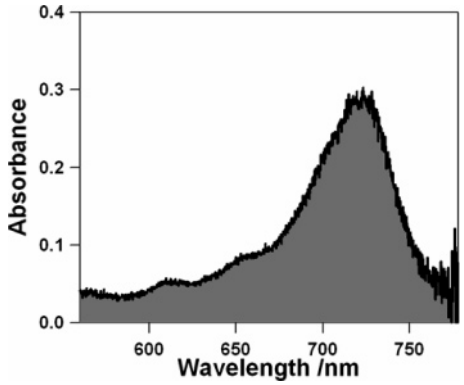

Figure 2. Typical absorption spectrum of the TPP J-aggregate microcrystal, which has been obtained by the illumination lamp attached to the microscope.

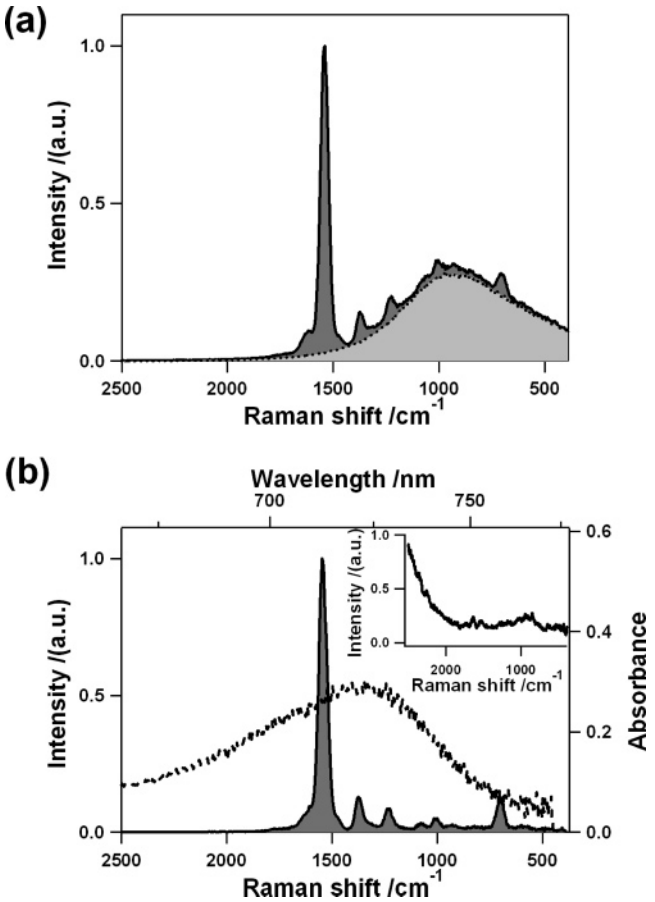

Figure 3. (a) CARS spectra at zero (solid, hatched by dark gray) and −13.3 ps (dotted, hatched by light gray) delay time between the pump and Stokes pulses; (b) Spectral profile of the corrected CARS signal (solid, hatched by dark gray), which is calculated by the subtraction of the CARS signal at the delay time of −13.3 ps from the CARS signal at zero delay time. The intensity correction of the CARS signal has been performed. Also shown is the spectral profile of the absorption signal (dotted). Spectral profile of the nonresonant CARS signal due to a cover glass is indicated in the inset.

temporal overlap between the pump and Stokes pulses. It is also noted that the negative delay means that the Stokes pulse follows the pump pulse. The spectral profile at the zero delay time shows many sharp features due to the CARS processes. In addition to these CARS signals, a broad feature is also observed around 1000 cm^{-1}. This signal is observed even when the pump and Stokes pulses are not temporally overlapped (−13.3 ps). Therefore, it is ascribed to the fluorescence from the TPP J-aggregate microcrystal. We have examined the excitation power dependence of this fluorescence signal. The excitation power dependence of the fluorescence signal is described by $I_{\mathrm{fluo}} \propto I_{\mathrm{pump}}^{1.05\pm0.08}$ without the Stokes laser. Here I_{fluo} and I_{pump} represent the intensities of the fluorescence and the pump pulses, respectively. Therefore, the fluorescence signal, which is observed at −13.3 ps, is caused by the one-photon process. Note that the wavelength of the pump pulse (800 nm) is slightly longer than that of the absorption peak (722 nm) of the J-aggregate microcrystal. We consider that the fluorescence is caused by the hot-band excitation, which is detectable due to the high fluorescence quantum yield of the J-aggregates. Figure 3b shows the CARS spectra, which is calculated by the subtraction of the CARS signal at the delay time of −13.3 ps from that at zero delay time. The intensity correction of the CARS signal has been performed using a CARS signal of a cover glass obtained by the same setup but at the different depth position. The peak positions observed in the CARS spectrum and their assignments are summarized in Table 1. It is known that the CARS signal at 700 cm^{-1}, which has not yet been assigned, is enhanced when the TPP molecules are aggregated.[11] Although similar peaks are found in the Raman spectrum of the monomer,[8,11] the CARS signal is not detected for a CH_2Cl_2 solution of TPP. It can be explained by the off-resonance electronic condition of the TPP monomer. Furthermore, no CARS signal is observed for aqueous sulfuric acid alone. Hence, it is concluded that the observed CARS signal originates from TPP J-aggregates. As shown in Figure 3b, a clear CARS signal is detected with a short exposure time (60 ms). Especially, the strong CARS signal due to the $C_\beta{=}C_\beta$ stretching mode is observed at 1544 cm^{-1}. Such an intense CARS signal originates from the strong excitonic resonance effect of the TPP J-aggregates. The absorption peak of the S_1-exciton state (Q-band) of TPP J-aggregates is about 722 nm. On the other hand, the center wavelength of the pump laser is about 800 nm, which is close to the absorption peak of the Q-band. In addition to the preresonance electronic condition of the pump laser, the CARS signal is generated in the wavelength region from 700 to 770 nm (See Figure 3b). In fact, it matches the absorption spectrum due to the Q-band, which is also depicted in Figure 3b. Therefore, both the CARS resonance and the pump preresonance conditions contribute to the enhancement of the CARS signal of TPP J-aggregates. It is also noted that the peak position in the CARS spectrum is slightly shifted in comparison with those of a small microcrystal.[25] It is considered to indicate the different crystalline condition of TPP monomer in the aggregation process. From an in-depth analysis of the spectral profile depicted in Figure 3b, a weak fluorescent signal due to the two-photon excitation is also found. The intensity ratio of the fluorescent signal due to the two-photon excitation to that due to the one-photon excitation is estimated to be about 10% from the signal at zero and −13.3 ps delay times. It will be discussed in subsection D.

TABLE 1: Band Positions and Assignments of TPP J-aggregates

Raman shift/cm^{-1}	assignment
700	?
1006	$\delta_{as}(C_\beta{-}H)$?
1075	$\delta_s(C_\beta{-}H)$
1232	C_m−phenyl
1373	$C_\alpha{-}N$ or $C_\alpha{-}C_\beta$
1544	$C_\beta{-}C_\beta$

B. Ultra-Broadband Multiplex CARS Imaging of a J-Aggregate Microcrystal. Thanks to the ultra-broadband multiplex CARS setup, we can reconstruct CARS images for multiple Raman bands with a simultaneous detection. Figure 4 shows the result of the CARS literal imaging of the J-aggregate microcrystal at six different Raman shifts. The CARS image does not change significantly for different Raman shifts. There are two common features in Figure 4. First, the intense CARS signal is observed especially at the top part of the microcrystal. Second, the right edge of the microcrystal gives a small CARS signal intensity. It is also noted that a relatively large CARS signal is observed at the bottom part of the microcrystal for the CARS image at the Raman shift of 700 cm^{-1} in comparison with the other five CARS images. Although the spectral coverage of the present setup is ranging from 360 to 3210 cm^{-1},[41] the CARS signal is not observed at the C−H or N−H stretching region. This tendency does not depend on the shape or size of the microcrystals.[25] It is likely that the CARS signals due to the C−H or N−H vibrational modes are not resonance

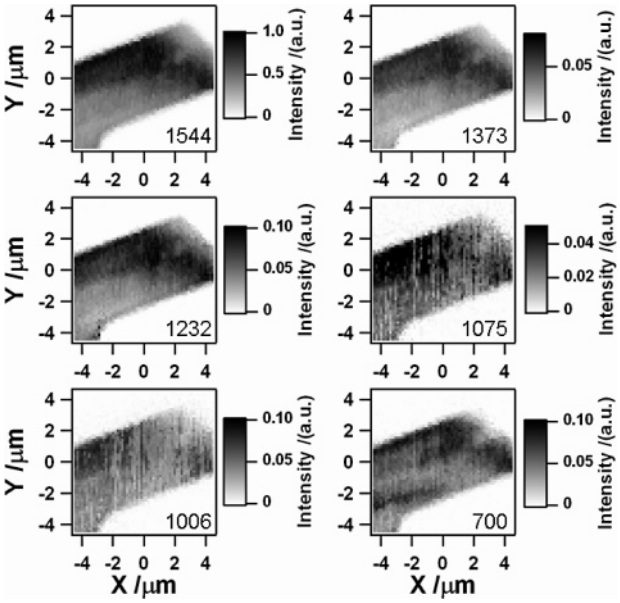

Figure 4. CARS literal images of the J-aggregate microcrystal at six different Raman shifts. The corresponding Raman shift is indicated at the bottom of each image.

enhanced because they are not much coupled with the $\pi^* \leftarrow \pi$ transition in resonance.

C. Three-Dimensional CARS Imaging of a J-Aggregate Microcrystal. Figure 5 shows a three-dimensional CARS image of a J-aggregate microcrystal at the Raman shift of 1544 cm^{-1}. Owing to the high three-dimensional spatial resolution due to the third-order nonlinear optical process, we can perform optical sectioning of the J-aggregate microcrystal. The piezo stage is scanned with a step of 0.46 μm in this experiment. The positive Z value corresponds to the upper part of the microcrystal on the cover glass, which is placed on the inverted microscope. As clearly observed in Figure 5, the CARS signal intensity at the top and bottom parts is large at the negative and positive Z values, respectively. It means that the microcrystal is slightly tilted.

D. One- and Two-Photon Excitation Fluorescence Imaging of a J-Aggregate Microcrystal. Figure 6a shows the fluorescence spectrum of the S_1-exciton state (Q-band). Owing to the high quantum yield of the TPP J-aggregates, the strong fluorescence signal is observed. Parts b and c of Figure 6 show the fluorescence images of the J-aggregate microcrystal at zero and −13.3 ps delay times, respectively, which are obtained by mapping the fluorescence intensity at 746 nm. Although the spatial resolution is poor compared with that of the CARS image, a clear spatial dependence is observed. Especially, the strong fluorescence signal is found at the right edge and the bottom part of the microcrystal. As discussed in subsection A, the intensity difference between the 0 and −13.3 ps delay time originates from the contribution of the fluorescence signal due to the two-photon excitation. Subtraction of the image in Figure 6c from that in Figure 6b enables us to obtain a two-photon excitation fluorescence (TPEF) image, which is shown in Figure 6d. The corresponding spectral profile is weakly observed in Figure 3b around 1000 cm^{-1}. Although the two-photon excitation spectrum has not yet been elucidated in this system, the two-photon excitation of water-soluble porphyrin J-aggregates has been investigated.[14,15] Taking account of the spectral coverage of the Stokes pulse, the two-photon allowed excited state is expected to exist in the range from 406 to 460 nm. In this region, the one-photon allowed second excited state (B band or Soret band) is also overlapped. Because the TPEF process is one of the third-order nonlinear optical processes, the spatial resolution is higher than that of the nonconfocal one-photon fluorescence microscopy. Although the spatial resolution is different, parts a−c indicate similar spatial dependence of

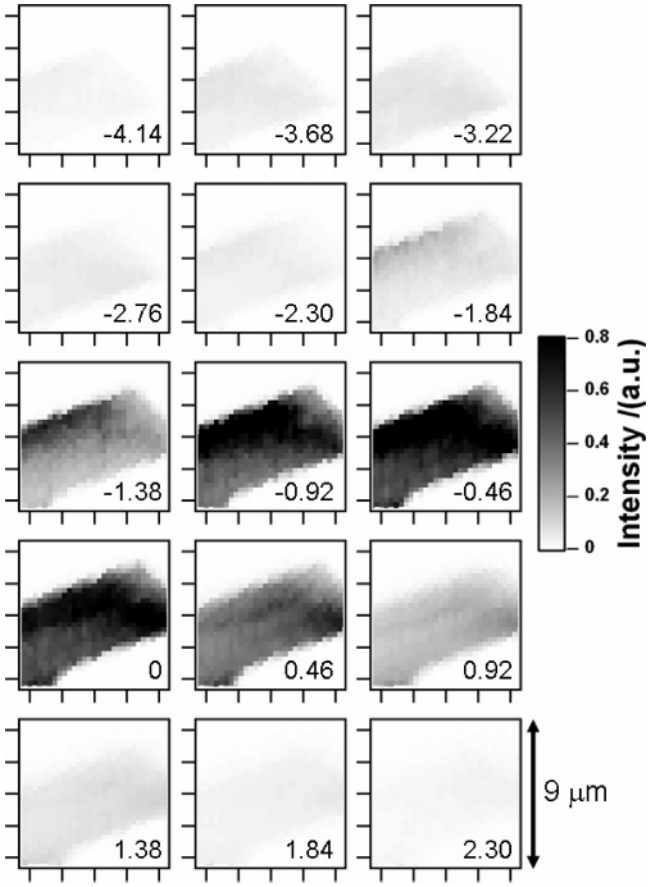

Figure 5. Three-dimensional CARS image of a J-aggregate microcrystal. The piezo stage is scanned with a step of 0.46 μm in the depth direction. The depth position is indicated as a micrometer scale in each image. The positive Z value corresponds to the upper part of the microcrystal on the cover glass, which is placed on the stage of the inverted microscope.

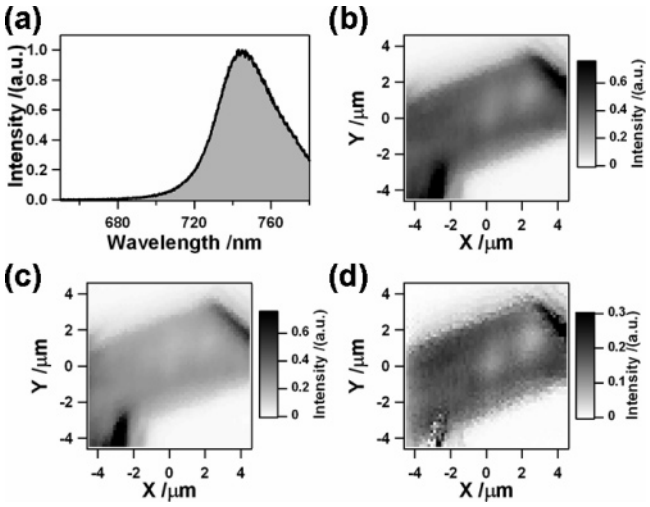

Figure 6. (a) Spectral profile of the fluorescence signal from the S_1-exciton state (Q-band); fluorescence image of the J-aggregate microcrystal at 0 (b) and −13.3 ps (c) delay time, respectively, which are obtained by mapping the fluorescence intensity at 746 nm; (d) two-photon excitation fluorescence (TPEF) image, which is calculated by the subtraction of the image in Figure 6c from that in Figure 6b.

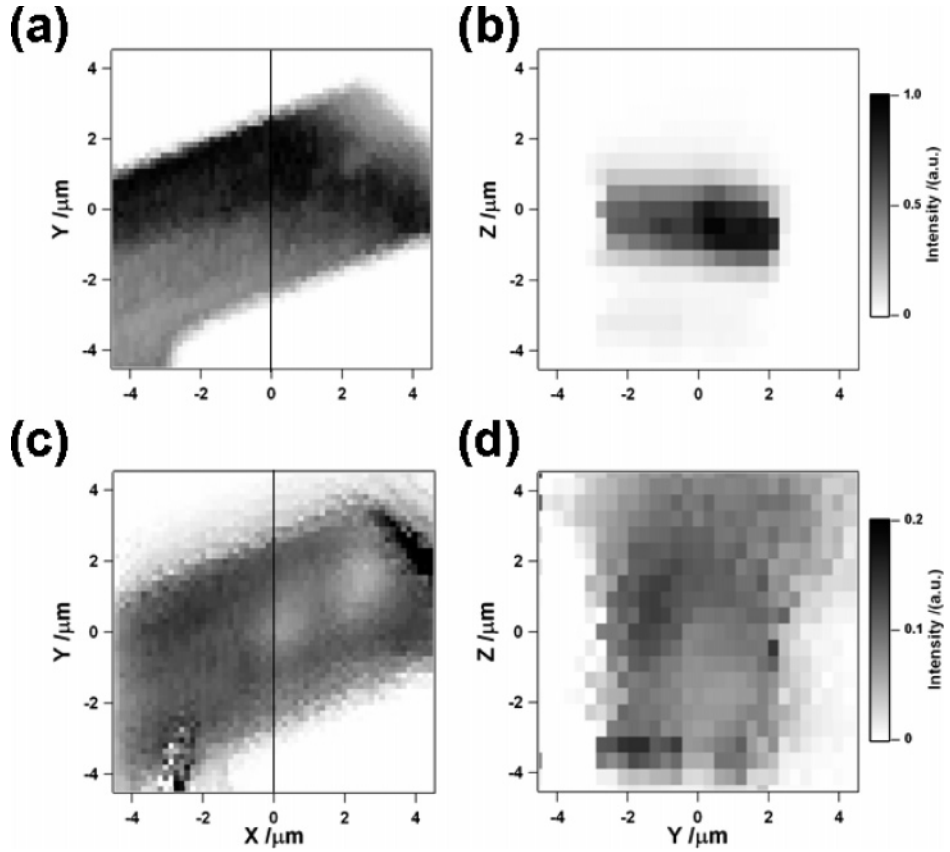

Figure 7. CARS and TPEF images of the J-aggregate microcrystal in lateral ($X-Y$) ((a) and (c), respectively) and axial ($Y-Z$) ((b) and (d), respectively) directions.

signals. As discussed in the one-photon fluorescence image, the right edge of the microcrystal gives a large TPEF signal. Furthermore, the TPEF signal decreases around $(x, y) = (2.6\ \mu m, 1.2\ \mu m)$ and $(x, y) = (0.5\ \mu m, 0.3\ \mu m)$. In fact, the CARS signal is relatively strong in these positions.

E. Multi-Nonlinear Optical Imaging of a J-Aggregate Microcrystal. Owing the high spatial resolution of the CARS and TPEF images, we can reconstruct three-dimensional CARS and TPEF images with simultaneous detection. Figure 7 shows both CARS and TPEF images of the J-aggregate microcrystal in lateral (X−Y) and axial (Y−Z) directions. As observed in Figure 7b, the microcrystal is slightly tilted along the Z axis. It agrees well with the result in Figure 5. Interestingly, the $Y-Z$ plot indicates that an area where the CARS signal is strong corresponds to an area where the TPEF signal is weak. This finding will be discussed later in detail. We have recently reported the CARS image of a small rod-shaped J-aggregate microcrystal.[25] The signal intensity from the small microcrystal due to the one- and two-photon excitation fluorescence is much smaller in comparison with the present study. The high quantum yield of fluorescence especially at the edge of the microcrystal could be explained by the well-oriented transition dipole moment in J-aggregates.

F. Comparison of the CARS Image with the Intensity, the Peak Position, and the Full-Width-at-Half-Maximum Images of the Fluorescence Signal. To investigate the apparently correlated CARS and TPEF images, we have analyzed the fluorescence signal in detail. Figure 8 shows the CARS image at the Raman shift of 1544 cm^{-1} (a), the one-photon fluorescence image at the intensity maximum at 746 nm (b), the peak-position (c) and the full-width-at-half-maximum (fwhm) (d) images of the one-photon fluorescence signal, respectively. Here we used the one-photon fluorescence signal rather than the TPEF signal because the spectral profile can be analyzed with a high signal-to-noise ratio. Taking account of the different spatial resolution between the CARS and one-photon fluorescence images, the intensity pattern of the CARS signal (Figure 8a) coincides well with the peak-position image (Figure 8c) rather than the fluorescence image. In other words, as the peak position of the fluorescence signal shifts to shorter wavelength, the CARS signal intensity becomes larger. On the other hand, the one-photon fluorescence image (Figure 8b) is in good agreement with the fwhm image (Figure 8d). Namely,

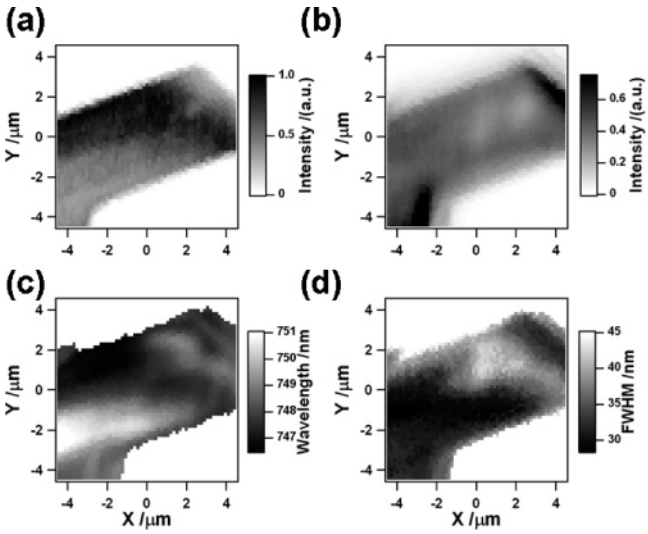

Figure 8. (a) CARS image at the Raman shift of 1544 cm^{-1}; (b) one-photon fluorescence image at the intensity maximum; peak-position (c) and full-width-at-half-maximum (fwhm) (d) images of the one-photon fluorescence signal, respectively.

as the fwhm increases, the fluorescence signal decreases in accordance with the change of fwhm.

These correlations between CARS and fluorescence images can be explained qualitatively by the excitonic coupling between the TPP monomers in J-aggregates. First, we shall discuss the correspondence between parts a and c of Figure 8. The excitonic transition is red-shifted in comparison with that of the monomer. Assuming a linear aggregate, the absorption energy shift due to the exciton coupling can be described by $2J$. Here, J corresponds to the transfer interaction matrix element for nearest neighbors,[46,47] and is written as follows,

$$J = \mu^2(1 - 3\cos^2\theta)/\hbar a^3 \quad (1)$$

Here μ, θ, and a correspond to the transition dipole moment of the TPP monomer, an angle of the transition dipole moment with respect to the aggregate axis, and a distance between the nearest monomers. J is negative in the case of J-aggregates. Therefore, the red shift is found in the absorption spectrum. Assuming that the intra- or interaggregate relaxation processes in the excited state do not differ significantly between each J-aggregate microcrystal, the peak position of the fluorescence spectrum is considered to be correlated to that of the absorption spectrum. As a consequence, the peak-position image of the fluorescence signal is expected to correspond to the peak-position image of the absorption signal, namely the image of the $|J|$ value. In other words, the large value of $|J|$ gives the fluorescence signal whose peak is positioned at longer wavelength. As shown in Figure 8c, the peak position of the fluorescence signal is located at a short/long wavelength in the top/the bottom part of the microcrystal. Therefore, the $|J|$ value is small/large in the top/the bottom part of the microcrystal, respectively. On the other hand, the spectral profile of the absorption signal is shown in Figure 3b. The peak position of the absorption signal is located at 722 nm, which is a slightly longer wavelength than that of the peak position of the CARS signal at 1544 cm^{-1} (713 nm). The CARS signal is strongly enhanced when the absorption peak coincides with that of the CARS signal due to the excitonic resonance effect. Therefore, as the absorption peak is shifted to shorter wavelength due to the weak excitonic coupling, the larger CARS signal is expected to be observed. In other words, the CARS signal intensity indicates the degree of the excitonic resonance effect through the energy shift of the excitonic coupling. The CARS resonance effect is expected to contribute to the signal much larger than the pump resonance effect, because the former and the latter are in just and in preresonance conditions, respectively.

Second, the correspondence between parts b and d of Figure 8 will be discussed. Assuming a linear aggregate, the transition dipole moment from the ground state to the one-exciton state with the wavevector of k, $\mu_{k\leftarrow G}$, is given by[46,47]

$$\mu_{k\leftarrow G} = \mu\sqrt{\frac{2}{N+1}}\frac{1-(-1)^k}{2}\cot\left[\frac{\pi k}{2(N+1)}\right] \quad (2)$$

Here N represents the number of aggregated TPP molecules, namely the coherence length (or delocalized size) of the exciton. The wavevector k is ranging from 1 to N. The exciton state with $k = 1$ contains the most oscillator strength, $0.81(N+1)\mu^2$. Therefore, the fluorescence intensity is approximately proportional to the factor of $N\mu^2$. On the other hand, the absorption spectrum should narrow by a factor of $\sqrt{N}$ due to a motional narrowing effect.[3] As discussed, the intensity of the fluorescence signal increases when the fwhm of the fluorescence signal decreases. Although the inhomogeneous broadening should also be taken into account, the experimental results shown in Figure 8b,d can be explained well by the variation of the coherence length of the exciton, N. Namely, the fluorescence intensity and fwhm is changed in accordance with the coherence length, N. Neglecting the inhomogeneity and intra- and interaggregate energy relaxation, the standard deviation of the coherence length δN is related to the standard deviation of the fwhm $\delta(\Delta\nu)$ as follows,

$$\frac{\delta(1/\sqrt{N})}{1/\sqrt{N}} = \frac{\delta(\Delta\nu)}{\Delta\nu} \quad (3)$$

Here $\Delta\nu$ is the fwhm of the fluorescence signal. $\delta(\Delta\nu)$ and $\Delta\nu$ are evaluated from the standard deviation and mean value of the fwhm shown in Figure 8d, respectively, and are determined to be $\delta(\Delta\nu) = 71$ cm^{-1} and $\Delta\nu = 612$ cm^{-1}. Substituting these values, $\delta N = 2N\cdot(\delta(\Delta\nu)/\Delta\nu)$ is evaluated to be $\delta N = 0.23N$. It means that the deviation of the coherence length is about 23% in the single J-aggregate microcrystal. In fact, J-aggregates are known to have a hierarchical structure.[48] A macroaggregate such as a microcrystal observed in the present study is composed of many "mesoaggregates", in which the exciton is fully delocalized. The spatial dependence of the coherence length can be explained by the different size of the mesoaggregates in the macroaggregate. Because the coherence length of the exciton can be estimated by evaluating the transition energy from the one- to two-exciton state,[49,50] time- and space-resolved ultrafast absorption spectroscopy is needed to elucidate the detailed hierarchical structure of the J-aggregates.

4. Conclusion

In conclusion, we have succeeded in visualizing a platelike porphyrin J-aggregate microcrystal using ultra-broadband multiplex CARS microspectroscopy. The strong CARS signal is observed due both to the CARS resonance and to the pump preresonance conditions. The three-dimensional CARS image allows us to investigate detailed crystalline structure of the J-aggregate microcrystal. On the basis of the comparison between the CARS and the fluorescence images, the spatial dependence of the CARS signal is explained by the spatial inhomogeneity of the excitonic transition energy of the J-aggregate microcrystal. The intensity, peak-position, and fwhm images of the fluorescence signal help us to elucidate in-depth excitonic property of the J-aggregate microcrystal. Because the spectral profile of the supercontinuum is spreading from the visible to near-infrared, it is also capable of obtaining the absorption image of the J-aggregate microcrystal. Combined analysis of CARS, fluorescence, and absorption images will provide more detailed information of crystalline structure of J-aggregates.

Acknowledgment. This research is supported by a Grant-in-Aid for Creative Scientific Research (No. 15GS0204) from the Ministry of Education, Culture, Sports, Science, and Technology of Japan. H.K. is supported by a Grant-in-Aid for Young Scientists (B) (No. 15750005) from Japan Society for the Promotion of Science, and research grants from The Kurata Memorial Hitachi Science and Technology Foundation. We thank Prof. Segawa for fruitful discussion.

References and Notes

(1) Davydov, A. S. *Theory of Molecular Excitons*; Plenum: New York, 1971.

(2) Kobayashi, T. *J-aggregates*; World Scientific Publishing: Singapore, 1996.
(3) Knapp, E. W. *Chem. Phys.* **1984**, *85*, 73.
(4) Fidder, H.; Knoester, J.; Wiersma, D. A. *Chem. Phys. Lett.* **1990**, *171*, 529.
(5) Pasternack, R. F.; Huber, P. R.; Boyd, P.; Engasser, G.; Francesconi, L.; Gibbs, E.; Fasella, P.; Venturo, G. C.; Hinds, L. d. C. *J. Am. Chem. Soc.* **1972**, *94*, 4511.
(6) Ohno, O.; Kaizu, Y.; Kobayashi, H. *J. Chem. Phys.* **1993**, *99*, 4128.
(7) Ribo, J. M.; Crusats, J.; Farrera, J. A.; Valero, M. L. *J. Chem. Soc., Chem. Commun.* **1994**, 681.
(8) Akins, D. L.; Zhu, H. R.; Guo, C. *J. Phys. Chem.* **1994**, *98*, 3612.
(9) Maiti, N. C.; Ravikanth, M.; Mazumdar, S.; Periasamy, N. *J. Phys. Chem.* **1995**, *99*, 17192.
(10) Akins, D. L.; Zhu, H.-R.; Guo, C. *J. Phys. Chem.* **1996**, *100*, 5420.
(11) Akins, D. L.; Ozcelik, S.; Zhu, H.-R.; Guo, C. *J. Phys. Chem.* **1996**, *100*, 14390.
(12) Mallamace, F.; Micali, N.; Trusso, S.; Monsu, L.; Scolaro, L. M.; Romeo, A.; Terracina, A.; Pasternack, R. F. *Phys. Rev. Lett.* **1996**, *76*, 4741.
(13) Maiti, N. C.; Mazumdar, S.; Periasamy, N. *J. Phys. Chem. B* **1998**, *102*, 1528.
(14) Misawa, K.; Kobayashi, T. *J. Chem. Phys.* **1999**, *110*, 5844.
(15) Kano, H.; Kobayashi, T. *J. Chem. Phys.* **2002**, *116*, 184 2002.
(16) Kano, H.; Saito, T.; Kobayashi, T. *J. Phys. Chem. A* **2002**, *106*, 3445.
(17) Kano, H.; Kobayashi, T. *Bull. Chem. Soc. Jpn.* **2002**, *75*, 1071.
(18) Okada, S.; Segawa, H. *J. Am. Chem. Soc.* **2003**, *125*, 2792.
(19) Gouterman, M.; Rentzepis, P.; Straub, K. D. *Porphyrins: Excited States and Dynamics*; American Chemical Society: Washington, DC, 1986.
(20) Nagahara, T.; Imura, K.; Okamoto, H. *Chem. Phys. Lett.* **2003**, *381*, 368.
(21) Nagahara, T.; Imura, K.; Okamoto, H. *Rev. Sci. Instrum.* **2004**, *75*, 4528.
(22) Akimov, D. A.; Ivanov, A. A.; Alfimov, M. V.; Grabchak, E. P.; Shtykova, A. A.; Petrov, A. N.; Podshivalov, A. A.; Zheltikov, A. M. *J. Raman Spectrosc.* **2003**, *34*, 1007.
(23) Guo, C.; Ren, B.; Akins, D. L. *J. Phys. Chem. B* **1998**, *102*, 8751.
(24) Ren, B.; Tian, Z. Q.; Guo, C.; Akins, D. L. *Chem. Phys. Lett.* **2000**, *328*, 17.
(25) Kano, H.; Hamaguchi, H. Vibrational imaging of a J-aggregate microcrystal using ultrabroadband multiplex coherent anti-Stokes Raman scattering microspectroscopy. *Vibrational Spectroscopy*, accepted.
(26) Zumbusch, A.; Holtom, G. R.; Xie, X. S. *Phys. Rev. Lett.* **1999**, *82*, 4142.
(27) Hashimoto, M.; Araki, T.; Kawata, S. *Opt. Lett.* **2000**, *25*, 1768.
(28) Cheng, J.-X.; Jia, Y. K.; Zheng, G.; Xie, X. S. *Biophys. J.* **2002**, *83*, 502.
(29) Mueller, M.; Schins, J. M. *J. Phys. Chem. B* **2002**, *106*, 3715.
(30) Schaller, R. D.; Ziegelbauer, J.; Lee, L. F.; Haber, L. H.; Saykally, R. J. *J. Phys. Chem. B* **2002**, *106*, 8489.
(31) Yakovlev, V. V. *J. Raman Spectrosc.* **2003**, *34*, 957.
(32) Paulsen, H. N.; Hilligsoe, K. M.; Thogersen, J.; Keiding, S. R.; Larsen, J. J. *Opt. Lett.* **2003**, *28*, 1123.
(33) Ichimura, T.; Hayazawa, N.; Hashimoto, M.; Inouye, Y.; Kawata, S. *Phys. Rev. Lett.* **2004**, *92*, 220801/1.
(34) Knutsen, K. P.; Johnson, J. C.; Miller, A. E.; Petersen, P. B.; Saykally, R. J. *Chem. Phys. Lett.* **2004**, *387*, 436.
(35) Cheng, J.-X.; Xie, X. S. *J. Phys. Chem. B* **2004**, *108*, 827.
(36) Kee, T. W.; Cicerone, M. T. *Opt. Lett.* **2004**, *29*, 2701.
(37) Kano, H.; Hamaguchi, H. *Appl. Phys. B* **2005**, *80*, 243.
(38) Kano, H.; Hamaguchi, H. *Appl. Phys. Lett.* **2005**, *86*, 121113.
(39) Kano, H.; Hamaguchi, H. *Opt. Express* **2005**, *13*, 1322.
(40) Petrov, I. G.; Yakovlev, V. V. *Opt. Express* **2005**, *13*, 1299.
(41) Kano, H.; Hamaguchi, H. Dispersion-compensated supercontinuum generation for ultrabroadband multiplex coherent anti-Stokes Raman scattering spectroscopy. *J. Raman Spectrosc.* **2006**, *37*, 411.
(42) Russell, P. *Science* **2003**, *299*, 358.
(43) Wadsworth, W. J.; Ortigosa-Blanch, A.; Knight, J. C.; Birks, T. A.; Man, T. P. M.; Russell, P. S. J. *J. Opt. Soc. Am. B* **2002**, *19*, 2148.
(44) Zheltikov, A. M. *J. Exp. Theo. Phys.* **2005**, *100*, 833.
(45) Rotomskis, R.; Augulis, R.; Snitka, V.; Valiokas, R.; Liedberg, B. *J. Phys. Chem. B* **2004**, *108*, 2833.
(46) Knoester, J. *Phys. Rev. A* **1993**, *47*, 2083.
(47) Knoester, J.; Spano, F. C. *Phys. Rev. Lett.* **1995**, *74*, 2780.
(48) Kobayashi, T.; Misawa, K. *J. Lumin.* **1997**, *72*−*74*, 38.
(49) Juzeliunas, G.; Knoester, J. *J. Chem. Phys.* **2000**, *112*, 2325.
(50) Spano, F. C. *Chem. Phys. Lett.* **1994**, *220*, 365.